Fluorescence from X Traps in C_{60} Single Crystals

W. Guss, J. Feldmann, and E. O. Göbel
Fachbereich Physik and Zentrum für Materialwissenschaften, Philipps-Universität, Renthof 5, D-35032 Marburg, Germany

C. Taliani
Istituto di Spettroscopia Molecolare, Consiglio Nazionale delle Ricerche, Via de' Castagnoli, I-40126 Bologna, Italy

H. Mohn, W. Müller, P. Häussler, and H.-U. ter Meer
Hoechst AG, Angewandte Physik, D-65926 Frankfurt, Germany
(Received 29 November 1993)

We show that low-temperature fluorescence spectra of large high-quality C_{60} single crystals are mainly composed of several, independent pairs of T_{1g} false origins. In analogy to the case of anthracene single crystals the series of emission bands can be interpreted in terms of exciton (Frenkel) emission from so-called X traps. Temperature dependent luminescence experiments support this interpretation.

PACS numbers: 78.55.Kz, 33.50.Dq, 33.70.−w, 61.46.+w

Since fullerenes have become available in macroscopic quantities, the physical and chemical properties of this novel material system have attracted significant attention. Because of its high symmetry and rigidity, the C_{60} molecule stands out among most other molecules and exhibits characteristic electronic and optical properties. Photoluminescence spectroscopy is one of the most powerful tools to investigate the optical properties of isolated C_{60} molecules and of crystalline C_{60}. Many groups have studied the photoluminescent properties of C_{60} molecules in solution [1,2] and of solid C_{60} in different morphologies such as films, polycrystalline powder [3–12], and single crystals [13]. However, different optical spectra have been reported even for nominally equal morphologies. Thus, the microscopic interpretation of the fluorescence spectra, in particular for the solid phase, has been controversial up to now. In this paper, we show that the differing optical spectra are a direct consequence of X-trap fluorescence from solid C_{60}.

For all C_{60} systems, fluorescence has been observed covering the spectral range from approximately 650 nm to 1 μm at low excitation intensities. The corresponding fluorescence quantum yields are approximately 10^{-5} for C_{60} in solution and 7×10^{-4} for solid C_{60} [2,5]. The low quantum yield is a consequence of the long radiative lifetime $\tau_{S_1\text{-}S_0}$ of the dipole-forbidden singlet exciton recombination and the fast transfer of excitons from singlet to triplet states (intersystem crossing). Accordingly, the temporal decay of the fluorescence is governed by the time constant $\tau_{S_1\text{-}T_1}\approx 1.2$ ns for the singlet-triplet transfer [14,15] and not by the radiative singlet exciton lifetime $\tau_{S_1\text{-}S_0}\approx 1.8$ μs.

Recently, Negri, Orlandi, and Zerbetto [16] were able to interpret the vibrational structure of the emission spectrum of *molecular C_{60} in solution* [2]. These authors showed that the fluorescence spectrum can be explained in a Herzberg-Teller scheme, i.e., the lowest singlet excited state T_{1g} acquires ungerade character from energetically higher T_{1u} states by adiabatic vibronic coupling and thus the optical S_1-S_0 transition becomes partially dipole allowed [16]. As a consequence, so-called false origins determine the peak positions in the fluorescence and absorption spectra of C_{60}. However, only two false origins (209 cm^{-1} separated from each other) originating from t_{1u} and h_u vibronic couplings have appreciable oscillator strengths and are expected to dominate the optical spectra. In addition, Negri, Orlandi, and Zerbetto [16] showed that the activities of gerade vibronic modes to induce progressions in the fluorescence spectrum are modest (a_g modes) or even negligible (h_g modes).

A comparison of the fluorescence spectra published so far for the various *solid C_{60} systems* [1–13] shows that the shapes of the spectra, peak intensities, and even peak positions are not identical for all systems. It therefore seems that interactions of C_{60} molecules with the particular environment influence the luminescent electronic states and/or that distinct chemical impurities themselves contribute to the luminescence spectrum [6,8]. For solid C_{60}, the number of spectrally resolvable peaks obviously depends on the morphology of the C_{60} material [1–13]. Therefore, only high-quality single crystals should allow us (i) to resolve the vibronic structure of the fluorescence spectrum of solid C_{60} and (ii) to understand the influence of defects, surfaces, and impurities on the C_{60} fluorescence spectrum in more detail.

In this Letter, we report photoluminescence studies on high-quality C_{60} single crystals. At low temperature, a series of well-resolved fluorescence lines is observed. The intensity distribution of the emission spectrum depends on temperature and on the spatial position on the crystals. We can interpret the data by assuming that the emission spectrum consists of several pairs of T_{1g} false origins each pair corresponding to a surface or a defect induced C_{60} X trap or to C_{60} bulk emission. These findings demonstrate that the optical properties of crystalline C_{60} exhibit similarities to other molecular crystals and provide a conclusive explanation for the different optical spectra reported so far.

C_{60} was produced by the carbon-arc method of Krätschmer and Huffman [17]. The fullerene containing

0031-9007/94/72(16)/2644(4)$06.00

soot was extracted and chromatographically purified by a proprietary process. The C_{60} used is 99.4% pure. This material was sublimed in an inert gas atmosphere to give crystals of 1–2 mm diameter. The thin films were sublimated from C_{60} in ultrahigh vacuum onto quartz substrates. To avoid oxygen contamination all C_{60} samples were kept under argon atmosphere before mounting them in an evacuated helium flow cryostat. The excitation photon energy is 2 eV and we use low excitation intensities of 1 mW focused to a spot size of approximately 100 μm in diameter. Low temperatures and low excitation intensities guarantee that polymerization effects are minimized.

The influence of the morphology of solid C_{60} on the emission spectrum is clearly seen in Figs. 1(a)–1(c), where normalized fluorescence spectra taken at $T=10$ K are shown for a C_{60} film (a), polycrystalline C_{60} powder (b), and for a C_{60} single crystal (c). The spectrum of the C_{60} film exhibits only two strongly broadened emission bands at approximately 730 and 810 nm. It is reasonable in the case of the film to assume that fluorescing C_{60} molecules are located in statistically varying environments leading to pronounced inhomogeneous broadening effects in the optical spectra. The number of resolvable fluorescence peaks drastically increases in the case of the polycrystalline powder and, in particular, for the single crystal. The series of well-resolved luminescence peaks for the single crystal is a consequence of reduced inhomogeneous broadening of the individual optical transitions. At present, it is not clear, whether the linewidth $\Gamma \approx 22$ meV (FWHM) for the fluorescence peaks in Fig. 1(c) is mainly due to inhomogeneous or homogeneous broadening. However, $\Gamma \approx 22$ meV is an upper limit for the homogeneous linewidth corresponding to a lower limit of 60 fs for the dephasing time $T_2 = 2\hbar/\Gamma_{hom}$. Recently, Brorson *et al.* [18] performed subpicosecond four-wave mixing experiments on a C_{60} film at low temperature in order to determine the dephasing time. However, they could only give an upper limit of $T_2 \approx 100$ fs. If we assume that the dephasing rate is not sensitive to different C_{60} morphologies, this together with the linewidth data yields a dephasing time T_2 between 60 and 100 fs for the lowest S_1-S_0 transition in solid C_{60} corresponding to a range of the spectral width from 13 to 22 meV for the homogeneous linewidth.

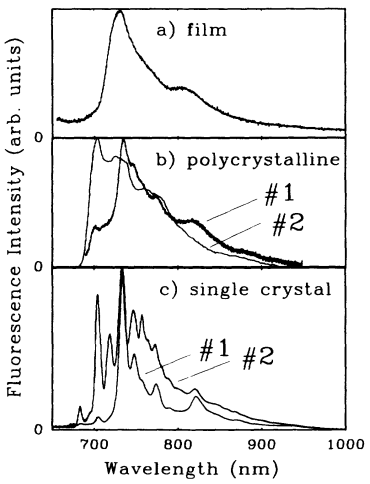

FIG. 1. Photoluminescence spectra taken at $T=10$ K for different morphologies of solid C_{60}: (a) C_{60} film, (b) polycrystalline C_{60} powder, and (c) C_{60} single crystal.

Spectrum 1 of Fig. 1(b) for polycrystalline C_{60} powder is taken from Ref. [9]. The spectrum peaks at approximately 730 nm and shows a similar but more structured shape than the fluorescence spectrum of the C_{60} film shown in Fig. 1(a). The fluorescence spectrum of the polycrystalline C_{60} material synthesized as described above is labeled 2 and peaks at approximately 703 nm, i.e., at shorter wavelengths than spectrum 1. In the case of the single crystal we also find differing spectra. The difference between spectrum 1 and spectrum 2 shown in Fig. 1(c) is only the spatial position of the laser excitation spot on the single crystal. This spatially inhomogeneous behavior of the fluorescence spectrum definitely shows that inhomogeneously distributed crystal imperfections such as chemical impurities or crystal defects influence the luminescence process. In a spatial scan over the crystal mostly spectra similar to the one labeled 1 in Fig. 1(c) are observed. In addition, such a spatial scan shows that a change in intensity for a particular fluorescence line is connected with a simultaneous change in intensity of a spectrally adjacent emission line. In other words, the spectrum seems to be composed of several pairs of emission lines spectrally separated by about 33 meV.

We state that each pair of fluorescence lines originates from C_{60} molecules in a particular crystal environment. The main line at approximately 732 nm is interpreted as fluorescence from C_{60} molecules located in a perfect C_{60} environment, i.e., it stems from bulk C_{60}. Other pairs of peaks are assigned to C_{60} molecules adjacent to chemical impurities, to crystal defects, or to crystal surfaces. The imperfect crystal environment induces an energetic shift of the electronic states and thus of the fluorescence of the particular C_{60} molecule. However, the defect does not change the characteristic vibronic structure of the fluorescence of the adjacent C_{60} host molecule. Such *defect-related luminescence from host molecules* is known for anthracene single crystals [19–21] and are called X traps.

As mentioned, Negri, Orlandi, and Zerbetto [16] showed that a pair of emission lines corresponding to 1437 cm^{-1} t_{1u}- and 1646 cm^{-1} h_u-related false origins are indeed expected to dominate the fluorescence spectrum of molecular C_{60}. The calculated spectral spacing between these two false origins is 26 meV [16], whereas the measured fluorescence spectrum of molecular C_{60} in solution provides a spacing of 31 meV [2,16] in good agreement with the observed spacings for the C_{60} single crystal in Fig. 1(c) (as shown below).

A more quantitative analysis of the single crystal

fluorescence data is presented in Fig. 2. The two spectra of Fig. 1(c) are redrawn in the upper parts. The pair of emission lines at 732 and 747 nm are assigned to the t_{1u}- and h_u-related false origins for bulk C_{60} emission. The fluorescence line at 821 nm is interpreted as a 1469 cm^{-1} totally symmetric a_g progression [3,5,12]. In Table I, the experimental values for the two false origins (t_{1u} and h_u) are listed in the second and third columns and in the row labeled C. In addition, the spectral spacing $\Delta \approx 34$ meV between the two experimentally observed t_{1u} and h_u false origins is given in the last column of Table I. Knowing the spectral positions of the t_{1u} and h_u false origins, the true 0-0 origin can be calculated [16]. We obtain 1.871 eV for the 0-0 origin as listed in the first column of Table I. This value must be compared to 1.893 eV for C_{60} molecules in solution [2,16]. The minor difference of 22 meV shows that band-structure effects mediated by van der Waals interaction [22,23] do not cause a pronounced redshift of the fluorescing excitonic transitions in solid C_{60}.

Three distinct pairs of emission lines corresponding to three distinct C_{60} X traps are clearly observed when scanning over the single crystal. These X traps are labeled X_1, X_2, and X_5 in Table I. The Δ values for these X traps are comparable to the one found for bulk C_{60} emission (compare with row C). There seem to be at least two more emission centers in the spectral range around 750 nm. However, their identification is more difficult since the corresponding false origin emission lines overlap. As can be seen in Table I we assume two further X traps, X_3 and X_4, to account for the intensity variations around 750 nm. Because of the spectral overlap we cannot directly identify the h_u-related fluorescence lines of the X_3 and X_4 traps from the spectra shown in Fig. 2. In order to gain more confidence in our assignment, we have tried to simulate the experimental spectra 1 and 2 shown in the upper parts of Fig. 2. For each emission center ($X_1, \ldots, X_5$, C) listed in Table I, we assume that only the t_{1u} and h_u false origins and the 1469 cm^{-1} a_g progression contribute to the fluorescence spectrum. For each emission center, the relative strengths of these three fluorescence lines are assumed to be 10:5:2. Taking into account a linewidth broadening of 22 meV for all emission lines, we then superimpose the "subspectra" of all emission centers listed in Table I. In order to account for the different spectral shapes of spectra 1 and 2, we vary the contribution, i.e., the overall strength of each subspectrum. The lower parts of Fig. 2 show two calculated fluorescence spectra constructed in such a way.

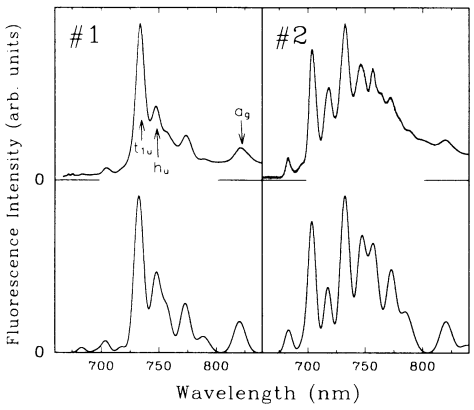

FIG. 2. Upper part: same experimental fluorescence spectra as shown in Fig. 1(c). Lower part: simulated fluorescence spectrum according to the model described in the text.

The main features of the experimentally observed spectra are well reproduced. Fluorescence spectra observed at other crystal positions (not shown in Figs. 1 and 2) can also be reproduced using our simple model. Discrepancies occur for wavelengths longer than ≈ 790 nm, since the observed long exponential tail into the near-infrared region [compare Fig. 1(c)] is not reproduced. Altogether, we find two X traps (X_1 and X_2) at higher photon energies and three X traps (X_3–X_5) at lower photon energies as compared to the energetic position of the bulk C_{60} emission (C). The fact that fluorescence from higher energy X traps (X_1 and X_2) can be observed means that excitation transfer from these X traps to, e.g., low-energetic bulk C_{60} molecules is hampered at low temperature. We attribute these X traps at higher energy to surface-related exciton states as is the case for crystalline anthracene [24,25]. The low-energetic X traps are due to C_{60} molecules around chemical impurities (residual solvent molecules, residual C_{70}, $C_{60}O_2$, polymerized C_{60}, etc.) and crystal defects (dislocations, vacancies, etc.).

In order to confirm our interpretation, we have studied the temperature dependence of the fluorescence spectrum of the C_{60} single crystal. In the temperature range from 10 K up to 100 K, we observe a drastic drop in intensity for the X_1- and X_2-related fluorescence lines, whereas the fluorescence intensities of all low-energetic emission lines exhibit no significant change in this temperature range. As can be seen in the inset of Fig. 3, the two fluorescence lines interpreted at t_{1u}- and h_u-related false origins of X trap X_2 both lose intensity and both show a slight blueshift with increasing temperature. This simultaneous behavior supports our interpretation that these two emission

TABLE I. List of emission centers (C: bulk C_{60}, X_i: X traps). The values for the two false origins, t_{1u} and h_u, are taken from the experimental fluorescence spectra, whereas the true origin 0-0 is calculated using the t_{1u} frequency from Ref. [16]. Δ is the spectral spacing between the two experimentally determined false origins.

	0-0	t_{1u}		h_u		Δ
	(eV)	(nm)	(eV)	(nm)	(eV)	(eV)
X_1	1.993	683.2	1.815	695.1	1.784	0.031
X_2	1.940	703.7	1.762	718.4	1.726	0.036
C	1.871	732.4	1.693	747.4	1.659	0.034
X_3	1.839	746.5	1.661	...	...	...
X_4	1.816	757.0	1.638	...	...	...
X_5	1.781	773.5	1.603	789.8	1.570	0.033

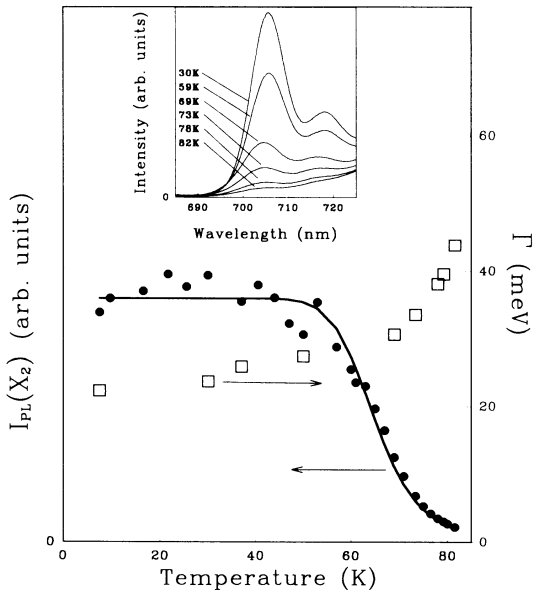

FIG. 3. Fluorescence intensity $I_{PL}(X_2)$ and linewidth Γ (FWHM) of the t_{1u}-related X_2 emission line at approximately 705 nm are plotted as a function of temperature as circles and squares, respectively. The inset shows the X_2-related fluorescence spectra for $T=30$, 59, 69, 73, 78, and 82 K.

lines originate from the same emission center and can be interpreted as the t_{1u}- and h_u-related false origins of X trap X_2. In Fig. 3, the luminescence intensity (circles) and the linewidth (FWHM) (squares) of the t_{1u}-related emission line at approximately 705 nm are plotted as a function of temperature. Up to $T\approx 50$ K, the fluorescence intensity remains virtually unchanged, but a further increase in temperature leads to a drastic drop in intensity. As already pointed out, the fast nonradiative singlet-triplet transfer ($\tau_{S_1\text{-}T_1}\approx 1.2$ ns) and the long radiative lifetime of the singlet exciton ($\tau_{S_1\text{-}S_0}\approx 1.8$ μs) determine the fluorescence efficiency at low temperatures. In order to quantitatively understand the temperature dependence of the fluorescence intensity, we assume that an additional temperature dependent nonradiative relaxation process [$\tau_{nr}(T)$] plays a role for the X_2-related fluorescence. The fact that the fluorescence related to bulk C_{60} emission (C) does not show this temperature induced drop in intensity justifies the assumption that $\tau_{S_1\text{-}T_1}$ and $\tau_{S_1\text{-}S_0}$ do not depend on temperature. Accordingly, the intensity of the X_2-related fluorescence, $I_{PL}(X_2)$, is assumed to obey

$$I_{PL}(X_2)\propto \tau_{S_1\text{-}S_0}^{-1}/[\tau_{S_1\text{-}S_0}^{-1}+\tau_{S_1\text{-}T_1}^{-1}+\tau_{nr}(T)^{-1}]. \quad (1)$$

Using experimental data and Eq. (1), we find that $\tau_{nr}(T)^{-1}$ exhibits an activated behavior:

$$\tau_{nr}(T)^{-1}=R_0\exp(-E_a/k_bT). \quad (2)$$

The solid line shown in Fig. 3 represents a fit of the experimental data by Eqs. (1) and (2) using $R_0=1.1\times 10^{15}$ s^{-1} and $E_a=78$ meV as parameters. We suggest that the activated nonradiative relaxation channel is due to intermolecular transfer of excitations from the surface related X_2 molecules to bulk C_{60} molecules.

As shown in Fig. 3, the linewidth of the X_2-related fluorescence line increases with increasing temperature. In particular, a drastic increase of the linewidth is observed for temperatures higher than 70 K, i.e., in the same temperature range, where the fluorescence intensity drastically drops. We therefore conclude that the temperature induced increase of the linewidth is correlated with the efficient nonradiative relaxation channel, i.e., with the intermolecular excitation transfer. Possibly, the ratcheting motion of the C_{60} molecules, which begins to occur at approximately 87 K, leads to an enhanced intermolecular excitation transfer.

We thank F. Zerbetto, U. Lemmer, S. T. Cundiff, P. Thomas, S. Baranovskii, H. Bässler, and R. Mahrt for helpful discussions and M. Preis for expert technical assistance. The work at Marburg University is financially supported by the Deutsche Forschungsgemeinschaft through the Leibniz Förderpreis.

[1] M. R. Wasielewski *et al.*, J. Am. Chem. Soc. **113**, 2774 (1991).
[2] Y. Wang, J. Phys. Chem. **96**, 764 (1992).
[3] C. Reber *et al.*, J. Phys. Chem. **95**, 2127 (1991).
[4] K. Pichler *et al.*, J. Phys. Condens. Matter **3**, 9259 (1991).
[5] P. A. Lane *et al.*, Phys. Rev. Lett. **68**, 887 (1992).
[6] M. Matus, H. Kuzmany, and E. Sohmen, Phys. Rev. Lett. **68**, 2822 (1992).
[7] S. P. Sibley, S. M. Argentine, and A. H. Francis, Chem. Phys. Lett. **188**, 187 (1992).
[8] T. Zhao *et al.*, Appl. Phys. Lett. **61**, 1028 (1992).
[9] J. Feldmann *et al.*, Europhys. Lett. **20**, 553 (1992).
[10] H. J. Byrne *et al.*, Appl. Phys. A **56**, 235 (1993).
[11] M. Diehl, J. Degen, and H. H. Schmidtke, Ber. Bunsenges. Phys. Chem. **97**, 908 (1993).
[12] E. Shin *et al.*, Chem. Phys. Lett. **209**, 427 (1993).
[13] Y. Iwasa, T. Koda, and S. Koda, Synth. Met. **55**, 3033 (1993).
[14] T. W. Ebbesen, K. Tanigaki, and S. Kuroshima, Chem. Phys. Lett. **181**, 501 (1991).
[15] M. Lee *et al.*, Chem. Phys. Lett. **196**, 325 (1992).
[16] F. Negri, G. Orlandi, and F. Zerbetto, J. Chem. Phys. **97**, 6496 (1992).
[17] W. Krätschmer and D. R. Huffman, Nature (London) **347**, 354 (1990).
[18] S. D. Brorson *et al.*, Phys. Rev. B **46**, 7329 (1992).
[19] A. Brillante *et al.*, Chem. Phys. Lett. **31**, 215 (1975).
[20] V. A. Lisovenko, M. T. Shpak, and V. G. Antoniuk, Chem. Phys. Lett. **42**, 339 (1976).
[21] D. P. Craig and J. Rajikan, J. Chem. Soc. Faraday Trans. 2 **74**, 292 (1978).
[22] S. Saito and A. Oshiyama, Phys. Rev. Lett. **66**, 2637 (1991).
[23] W. Y. Ching *et al.*, Phys. Rev. Lett. **67**, 2045 (1991).
[24] M. S. Brodin, M. A. Dudinskii, and S. V. Marisova, Opt. Spectrosc. **34**, 651 (1973).
[25] M. R. Philpott and J. M. Turlet, J. Chem. Phys. **64**, 2852 (1976).